

Online Ultrasound Sensor Calibration Using Gradient Descent on the Euclidean Group

Martin Kendal Ackerman[†], Alexis Cheng[‡], Emad Boctor[‡], Gregory Chirikjian[†]

Abstract

Ultrasound imaging can be an advantageous imaging modality for image guided surgery. When using ultrasound imaging (or any imaging modality), calibration is important when more advanced forms of guidance, such as augmented reality systems, are used. There are many different methods of calibration, but the goal of each is to recover the rigid body transformation relating the pose of the probe to the ultrasound image frame. This paper presents a unified algorithm that can solve the ultrasound calibration problem for various calibration methodologies. The algorithm uses gradient descent optimization on the Euclidean Group. It can be used in real time, also serving as a way to update the calibration parameters on-line. We also show how filtering, based on the theory of invariants, can further improve the online results. Focusing on two specific calibration methodologies, the $AX = XB$ problem and the $BX^{-1}p$ problem, we demonstrate the efficacy of the algorithm in both simulation and experimentation.

1. INTRODUCTION

In the modern robotic surgical setting, image-guided surgery (IGS) systems can be an important component, providing additional informational support and guidance [1–3]. An IGS system usually consists of several integrated elements such as an imaging modality system, a pose tracker, and the surgical robot. Of these systems, the medical imaging element provides a visualization of underlying tissue structures or anatomy that cannot

This work was supported by NSF Grant RI-Medium: 1162095

[†]Martin Kendal Ackerman and Gregory Chirikjian are with the Department of Mechanical Engineering and Laboratory for Computational Sensing and Robotics, Johns Hopkins University, Baltimore, MD, USA, gregc at jhu.edu

[‡]Alexis Cheng and Emad Boctor are with the Department of Computer Science and Radiology, and Laboratory for Computational Sensing and Robotics, Johns Hopkins University, Baltimore, MD, USA, eboctor1 at jhmi.edu

be seen with the naked eye. There are many popular imaging modalities, such as x-ray, computed tomography (CT), or magnetic resonance imaging (MRI), but this paper specifically focuses on ultrasound (US) imaging which has several notable advantages. US systems tend to be more mobile, use non-ionizing radiation, are lower in cost, and provide real-time data acquisition. With these important characteristics, US is frequently integrated with tracking systems and robotic systems for IGS.

When using US imaging (or any imaging modality), calibration is important when more advanced forms of guidance, such as augmented reality systems, are used. There are many different methods of calibration, but the goal of each is to recover the rigid body transformation relating the pose of the probe to the US image frame [4–7]. To accomplish this, a tracked rigid body must be attached to the US transducer. An external tracker is then used to obtain the tracked rigid body's pose within the external tracker's space. Additionally, some model (usually called a phantom) with known shape must be imaged to generate transformations in reference to the image frame. The choice of the type of phantom used is largely related to the calibration methodology, of which there are many.

The goal of this paper is to present an algorithm that can solve the US calibration problem for various calibration methodologies. The algorithm uses a gradient descent optimization, of an appropriate cost function, on the Euclidean Group ($SE(3)$ - the manifold of rigid body motions with the operation of composition). We also show how this algorithm can be used in real time, to serve as a way to update the calibration parameters on-line. In this way, any deviations of this system since the last calibration, as well as any in situ disturbances, can be accounted for. Finally we show how filtering can further improve the online results. The paper focuses on two specific calibration methodologies, the " $AX = XB$ " problem and the " $BX^{-1}p$ "

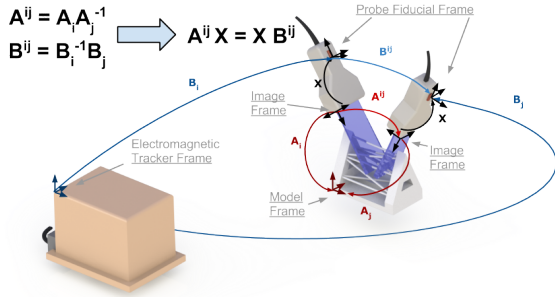


Figure 1. Defining Reference Frames for the $AX = XB$ Problem in Ultrasound

problem, to demonstrate the efficacy of the algorithm, however it could be applied to a variety of methodologies as long as an appropriate cost function is formulated.

The remainder of this section is devoted to reviewing the literature, and establishing notation. Section 2 outlines the gradient descent algorithm and Section 3 discusses a special filtering method for the $AX = XB$ case that uses the SE(3) geometric invariants. Section 4 uses simulated results to demonstrate the baseline efficacy of the algorithm. Section 5 demonstrates using the algorithm with two possible cost functions.

1.1. Literature Review

The problem of solving for sensor calibration parameters has a rich history. Although there are various methods of US calibration, this paper focuses on two specific formulations.

1.2. $AX = XB$ US Calibration

In many instances the sensor calibration problem can be written as:

$$AX = XB \quad (1)$$

where, A , X , and B are each homogeneous (rigid body) transformations with A and B given from sensor measurements, and X unknown (see Fig. 1). This problem has a history that goes back more than a quarter of a century, and applications involving this problem remain active today [6–10].

The rigid-body transformation X is required in order to properly accumulate 2D ultrasound images to form 3D image volumes. It is also needed for augmented reality applications where ultrasound images are fused with camera video images. More advanced US technologies such as

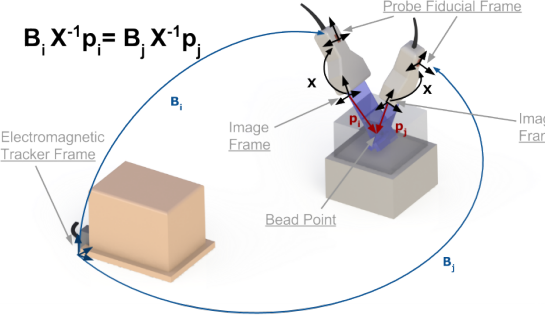


Figure 2. Defining Reference Frames for the $BX^{-1}p$ Problem in Ultrasound

tracked US elastography [3] also require X .

As pointed out in [6, 9, 10], there are two unspecified degrees of freedom in X constrained by (1), and a unique X cannot be found unless additional measurements are taken. This situation is rectified by considering two sets of exact measurements of the form in (1), i.e.,

$$A^{ij_1} X = XB^{ij_1} \quad \text{and} \quad A^{ij_2} X = XB^{ij_2}$$

and using methods in [6, 9, 10], provided some mild conditions are observed for the selection of the pairs (A^{ij_1}, B^{ij_1}) and (A^{ij_2}, B^{ij_2}) .

1.3. $BX^{-1}p$ US Calibration

The $BX^{-1}p$ problem is another formulation of a sensor calibration problem [5, 11, 12]. A phantom with a single embedded fiducial is imaged by a tracked US transducer in different poses. B and X are again homogeneous transformations with B given directly from sensor measurements, and X unknown. p is the physical point within the sensor's coordinate system (see Fig. 2). The relationship $B_i X p_i = B_j X p_j$ holds for all pairs of (B_i, B_j) since they are all measurements of the same physical point.

This formulation has been used for ultrasound crosswire calibration [11, 12] and tracked needle pivot calibration [5, 13]. The literature shows that this formulation also faces the same limitation in that a single pair satisfying

$$B_i X p_i = B_j X p_j \quad (2)$$

is insufficient in solving for a unique solution X . At least three independent poses (B_i, B_j, B_k) are required to generate three equations:

$$B_i X p_i = B_j X p_j$$

$$\begin{aligned} B_j X p_j &= B_k X p_k \\ B_k X p_k &= B_i X p_i \end{aligned}$$

However for any of the formulations, if there is sensor error, then it may not be possible to find compatible pairs that reproduce the exact value of the calibration parameters (e.g. X in $AX = XB$ or $B_i X p_i = B_j X p_j$). For this reason, minimization approaches are often taken where for $n > 2$ a cost function

$$C(X) = \sum_{i=1}^n w_i d^2(Y_1, Y_2) \quad (3)$$

is computed for some distance metric $d(\cdot, \cdot)$ on $SE(3)$. A wide variety of such metrics are discussed in [14] that have the useful property of left-invariance, $d(H_0 H_1, H_0 H_2) = d(H_1, H_2)$ for any $H_0, H_1, H_2 \in SE(3)$. The set $\{w_i\}$ consists of weights which can be taken to be a partition of unity. Quantities Y_1 and Y_2 are the appropriate quantities from the calibration equations (e.g. $Y_1 = A^{ij} X$, $Y_2 = X B^{ij}$, for $AX = XB$).

Perhaps the simplest of the left-invariant metrics is based on the weighted Frobenius norm

$$d^2(H_1, H_2) = \|\Delta H\|_W^2 = \text{trace}[(\Delta H) W (\Delta H)^T]$$

where $\Delta H = H_1 - H_2$ and W is a matrix that weights rotations and translations appropriately, as described in [14]. The sets of pairs (A_i, B_i) for $i = 1, 2, \dots, n$ is chosen such that the set $\{A_i\}$ is spread out over a variety of positions and orientations, and likewise for $\{B_i\}$, so that the resulting X is robust to measurement errors.

Finding X that minimizes (3) is reasonable for obtaining a single consensus value that approximately solves (1), and a large literature on this exists [6,8–10]. Our method uses such a cost function formulation and gives an algorithm that can be updated online, allowing new data to be used in real time to yield a better update of X . Additionally, each separate pair of sensor measurements can be treated somewhat independently, allowing the algorithm to use data of lower noise.

1.4. Notation

Let $H \in SE(3)$. Then

$$H = \begin{pmatrix} R & \mathbf{t} \\ \mathbf{0}^T & 1 \end{pmatrix} \quad \text{and} \quad H^{-1} = \begin{pmatrix} R^T & -R^T \mathbf{t} \\ \mathbf{0}^T & 1 \end{pmatrix}$$

are respectively a 4×4 homogeneous transformation matrix and its inverse. Such matrices describe a rigid-body motion, or pose, consisting of

a 3×3 rotation matrix and 3×1 translation vector \mathbf{t} . Here $\mathbf{0}^T$ is a 1×3 row of zeros. Multiplication of homogeneous transformations corresponds to concatenation of rigid-body motions, and $HH^{-1} = H^{-1}H = \mathbb{I}_4$, where \mathbb{I}_n denotes the $n \times n$ identity matrix. The set of all homogeneous transformations together with the operation of matrix multiplication defines the special Euclidean group, $SE(3)$.

The set of all 3×3 rotation matrices together with the operation of matrix multiplication constitutes the special orthogonal group, $SO(3)$. Any $R \in SO(3)$ can be written as [15]

$$R = e^{\theta N} = \mathbb{I}_3 + \sin \theta N + (1 - \cos \theta) N^2$$

where $e^{\theta N}$ denotes the matrix exponential, $\theta \in [0, \pi]$ is the angle of rotation and

$$N = \begin{pmatrix} 0 & -n_3 & n_2 \\ n_3 & 0 & -n_1 \\ -n_2 & n_1 & 0 \end{pmatrix}$$

where $\mathbf{n} \in \mathbb{R}^3$ is the unit vector describing the axis of rotation, which connects the origin and any point on the unit sphere.

2. The Gradient Descent Algorithm

Given a function $f : \mathbb{R}^n \rightarrow \mathbb{R}$ that is well defined and differentiable in a neighborhood of a point \mathbf{p} , the direction towards a local minimum that achieves the maximal rate of descent is found by the negative gradient of the function at the point \mathbf{p} . The minimum can be approached by taking a step, of a defined size α ($\alpha > 0$), along the negative gradient:

$$\mathbf{p}_{s+1} = \mathbf{p}_s - \alpha \nabla f(\mathbf{p}_s). \quad (4)$$

When $f(\cdot)$ is convex, ∇f is Lipschitz and α is chosen in an appropriate manner, it can be guaranteed that stepping in this manner will converge to a global minimum.

There is a natural extension of the concept of directional derivatives in \mathbb{R}^n to functions on a Lie group. To our knowledge, the first time this was used in the robotics field was in [16], and it has subsequently been used in a variety of applications [17, 18]. Let $X \in \mathcal{G}$, the Lie algebra corresponding to the group $G = SE(3)$, and let $f : G \rightarrow \mathbb{R}$ be an analytic function, where $g \in G$. Two forms of directional derivatives, the “right” and “left” Lie derivatives, can be defined as [15]

$$(\tilde{X}^r f)(g) \doteq \frac{d}{dt} f(g \circ \exp(tX)) \Big|_{t=0} \quad (5)$$

and

$$(\tilde{X}^l f)(g) \doteq \frac{d}{dt} f(\exp(-tX) \circ g) \Big|_{t=0}. \quad (6)$$

Without loss of generality, the definition of the right Lie derivative (5) can be used to define a gradient on $SE(3)$ using the standard basis of the Lie algebra, $\{E_i\}$ (for $i = 1, 2, \dots, 6$) [15], as our \tilde{X}^r operator.

$$\nabla f(g) = \begin{bmatrix} \frac{d}{dt} f(g \circ \exp(tE_1)) \Big|_{t=0} \\ \frac{d}{dt} f(g \circ \exp(tE_2)) \Big|_{t=0} \\ \vdots \\ \frac{d}{dt} f(g \circ \exp(tE_6)) \Big|_{t=0} \end{bmatrix}. \quad (7)$$

Using the concept of rigid body velocity, as defined by $V_g^r = g^{-1}\dot{g}$, we can write a differential equation for our time evolving calibration parameter.

$$g_{s+1} \approx g_s \exp(\Delta t V_g^r) \quad (8)$$

where time is measured in discrete steps of the form $s+1 = s\Delta t$ and Δt is a small timestep. If we define

$$V_g^r = g^{-1}\dot{g} = -\alpha \widehat{\nabla f(g)}, \quad (9)$$

where $\widehat{\cdot}$ assigns a 4×4 screw matrix to any 6-vector as in [20], equation (8) now becomes our update step, the analog of (4).

Defining the algorithm in this manner, we now have a tool that can solve a variety of problems that involve calibration on the Euclidean Group. This is done by letting $f(g)$ be an appropriate cost function for the particular calibration problem and iterating (8). As an example, for the $AX = XB$ problem, we can define a cost function as

$$C_{AX=XB} = \|A^{ij}X - XB^{ij}\|_W \quad (10)$$

and, similarly, for the $B_i X p_i = B_j X p_j$ problem we can define the cost function as

$$C_{BXp} = \|B_i X^{-1} p_i - B_j X^{-1} p_j\|_W. \quad (11)$$

3. Filtering for $AX = XB$

Given the $AX = XB$ calibration problem, we can perform additional filtering on the incoming data to choose A 's and B 's that are most suitable to solve the calibration (and reject pairs with large noise). In addition, situations where there arise high levels of noise, the user can be alerted and they can take steps to correct any faults.

Start by writing the problem as $A = XBX^{-1}$. Since this is a similarity transformation, the immediate implication is that each matrix invariant of A must be equal to the corresponding invariant of B . Moreover, it can be shown that all four of the matrix invariants for a homogeneous transformation either depend on θ , or are constant (e.g., $\text{tr}H = 2\cos\theta + 2$ and $\det H = 1$). However, as discussed in [19], the added group-theoretic structure of $SE(3)$ provides an additional invariant that is not immediately apparent from basic linear algebra. Further, as discussed in [20] there are two additional geometric invariants related to sets of (A, B) pairs.

As discussed in [20], explicitly calculating and equating the matrix product gives two invariant relations,

$$\theta_{A^{ij}} = \theta_{B^{ij}} \quad d_{A^{ij}} = d_{B^{ij}} \quad (12)$$

where $\theta_{A^{ij}}$ ($d_{A^{ij}}$) and $\theta_{B^{ij}}$ ($d_{B^{ij}}$) are computed from A^{ij} and B^{ij} respectively. For the additional two invariants, let

$$\mathbf{l}_{A^{ij}}(t) = \mathbf{p}_{A^{ij}} + t\mathbf{n}_{A^{ij}} \quad \text{and} \quad \mathbf{l}_{B^{ij}}(t) = \mathbf{p}_{B^{ij}} + t\mathbf{n}_{B^{ij}}$$

be the directed screw axis lines of A^{ij} and B^{ij} in three-dimensional Euclidean space. If the lines are not parallel or anti-parallel, i.e., if $\mathbf{n}_{A^{ij}} \neq \pm \mathbf{n}_{B^{ij}}$, then the distance between the two lines is given by [20]

$$\Delta(\mathbf{l}_{A^{ij_1}}, \mathbf{l}_{A^{ij_2}}) = \frac{\|[\mathbf{n}_{A^{ij_1}}, \mathbf{n}_{A^{ij_2}}, \mathbf{p}_{A^{ij_2}} - \mathbf{p}_{A^{ij_1}}]\|}{\|\mathbf{n}_{A^{ij_1}} \times \mathbf{n}_{A^{ij_2}}\|} \quad (13)$$

where for any $\mathbf{a}, \mathbf{b}, \mathbf{c} \in \mathbb{R}^3$, the triple product is $[\mathbf{a}, \mathbf{b}, \mathbf{c}] \doteq \mathbf{a} \cdot (\mathbf{b} \times \mathbf{c})$. In the current context we can think of $i_1 = 1$ and $i_2 = 2$ but in later discussion i_1 and i_2 can represent more general values. If in addition, $\Delta(\mathbf{l}_{A^{ij_1}}, \mathbf{l}_{A^{ij_2}}) \neq 0$, i.e., if the lines are skew, then the angle $\phi(\mathbf{l}_{A^{ij_1}}, \mathbf{l}_{A^{ij_2}}) \in [0, 2\pi)$ is uniquely specified by

$$\cos \phi(\mathbf{l}_{A^{ij_1}}, \mathbf{l}_{A^{ij_2}}) = \mathbf{n}_{A^{ij_1}} \cdot \mathbf{n}_{A^{ij_2}} \quad (14)$$

$$\sin \phi(\mathbf{l}_{A^{ij_1}}, \mathbf{l}_{A^{ij_2}}) = \Delta(\mathbf{l}_{A^{ij_1}}, \mathbf{l}_{A^{ij_2}})^{-1} [\mathbf{n}_{A^{ij_1}}, \mathbf{n}_{A^{ij_2}}, \mathbf{p}_{A^{ij_2}} - \mathbf{p}_{A^{ij_1}}].$$

If $\theta_{A^{ij_1}}, \theta_{A^{ij_2}} \in (0, \pi)$ and $\phi(\mathbf{l}_{A^{ij_1}}, \mathbf{l}_{A^{ij_2}}) \notin \{0, \pi\}$, then a unique solution of (1) exists if and only if the following four conditions hold:

1. $\theta_{A^{ij_1}} = \theta_{B^{ij_1}}$ and $\theta_{A^{ij_2}} = \theta_{B^{ij_2}}$;
2. $d_{A^{ij_1}} = d_{B^{ij_1}}$ and $d_{A^{ij_2}} = d_{B^{ij_2}}$;
3. $\phi(\mathbf{l}_{A^{ij_1}}, \mathbf{l}_{A^{ij_2}}) = \phi(\mathbf{l}_{B^{ij_1}}, \mathbf{l}_{B^{ij_2}})$;
4. $\Delta(\mathbf{l}_{A^{ij_1}}, \mathbf{l}_{A^{ij_2}}) = \Delta(\mathbf{l}_{B^{ij_1}}, \mathbf{l}_{B^{ij_2}})$.

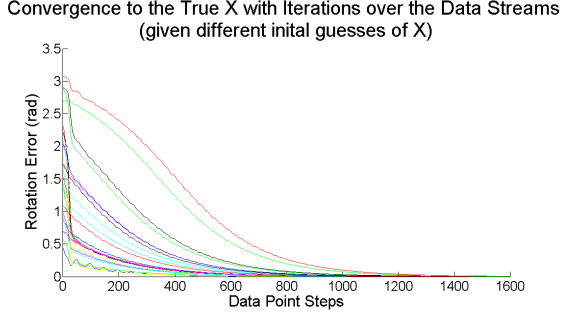


Figure 3. Validation using Simulated Results

If these do not hold, then a solution will not be possible [20].

If there is noise present in the data, then these four invariants generally will not exactly equal. However, one can filter the data based on these invariants and discard pairs (A^{ij}, B^{ij}) for which the difference in the invariants are too large. Examples of filtering functions using each of the four invariants

1. $diff_{\theta^{ij}} = |\theta_{A^{ij}} - \theta_{B^{ij}}| > thresh_{\theta^{ij}}$: discard (A^{ij}, B^{ij}) ;
2. $diff_{d^{ij}} = |d_{A^{ij}} - d_{B^{ij}}| > thresh_{d^{ij}}$: discard (A^{ij}, B^{ij}) ;
3. if $diff_{\phi^{ij}} = |\phi(\mathbf{l}_{A^{ij}}, \mathbf{l}_{A^{ik}}) - \phi(\mathbf{l}_{B^{ij}}, \mathbf{l}_{B^{ik}})| > thresh_{\phi^{ij}}$ for a majority of k : discard (A^{ij}, B^{ij}) ;
4. if $diff_{\Delta^{ij}} = |\Delta(\mathbf{l}_{A^{ij}}, \mathbf{l}_{A^{ik}}) - \Delta(\mathbf{l}_{B^{ij}}, \mathbf{l}_{B^{ik}})| > thresh_{\Delta^{ij}}$ for a majority of k : discard (A^{ij}, B^{ij}) .

Another possibility would be to combine the filtering with the gradient descent method in a more direct manner. For example, we can write the update step for each (A^{ij}, B^{ij}) pair as

$$g_{s+1} = g_s \exp(-\beta_{ij} \Delta t \widehat{\nabla f(g)}) \quad (15)$$

where $\beta_{ijk} = f(diff_{\theta^{ij}}, diff_{d^{ij}}, diff_{\phi^{ij}}, diff_{\Delta^{ij}}) \in (0, 1]$ such that β_{ij} approaches unity as the invariants become equal. For example, if the cost used is (10), we might only use $diff_{\theta^{ij}}$ and $diff_{d^{ij}}$ and let $\beta_{ij} = \exp(diff_{\theta^{ij}} \cdot diff_{d^{ij}})$. In this way we bias the gradient descent algorithm against stepping in directions given by pairs of data with high noise.

4. Verifying the Gradient Descent Algorithm with Simulation

To validate the efficacy of the gradient decent algorithm we simulated an $AX = XB$ calibration. Given a set of trajectories, B and A data streams were generated according to an a priori chosen

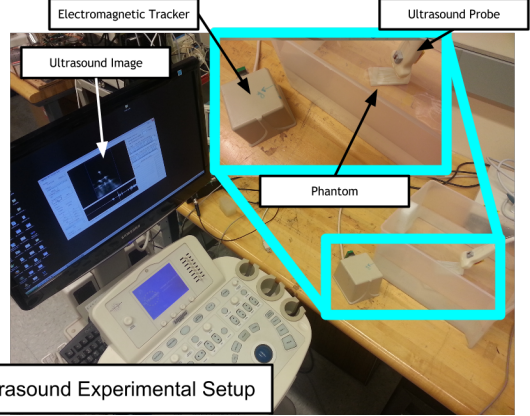


Figure 4. Ultrasound Experimental Setup

X. Since we must use relative motions, we generate $B^{ij} = B_i^{-1} B_{i+1}$ where B_i 's are drawn from two sample "s-shaped" trajectories on a sphere. After forming relative motions, B_{ij} 's, we calculate $A^{ij} = XB_iX^{-1}$, where X is the a priori chosen value.

Figure 3 shows the convergence to a solution as the algorithm iterates over points in the data stream, given multiple random initial guesses for X . It can be noted that since the algorithm converges much faster for a "good" initial guess of X , it could be used to update the knowledge of X on-line. In other words, in addition to solving for X given initial calibration data, the algorithm can be used to 1) "sharpen" X , given additional clean data, or 2) can be for the case where X has changed, due to any of the factors previously discussed. If the previously solved X is used in the online update, the convergence is rapid. The figure is representative, as it shows only the converging rotation error for $C_{AX=XB}$. For the translation error, and for $C_{BX^{-1}p}$, the performance is very similar.

5. Experimental Results of the Gradient Descent Algorithm

To show that our gradient descent algorithm was feasible for both of our cost functions on experimental data, we performed both an $AX = XB$ calibration and a $BX^{-1}p$ calibration. In the first case, we used the phantom shown in Fig. 4 and an electromagnetic tracker to collect pairs of A and B . In the second case, we used a phantom with a single embedded metal fiducial and an electromagnetic tracker to collect pairs of B and p . We examined the accuracy of the computed X by performing a reconstruction of the phantom model.

This can be done by computing $B_i X^{-1} p_i$ where p_i are the segmented model points in the first case, and the segmented bead in the second case. We quantify the reconstruction by fitting the model to the new computed point set and finding a normalized metric. (The data that was used in the experimental results can be obtained at <https://sourceforge.net/p/jhu-axxb/>)

In the $AX = XB$ case, for each point, we found its closest point on the model and computed the sum squared difference between them. In the $BX^{-1} p$ case, we compute the sum squared difference between each point and the mean of the point set. The mean and standard deviation of the sum squared differences was $1.62\text{mm} \pm 1.28\text{mm}$ and $1.52\text{mm} \pm 1.13\text{mm}$ in the unfiltered and filtered $AX = XB$ case respectively and $1.06\text{mm} \pm 0.48\text{mm}$ in the $BX^{-1} p$ case

6. CONCLUSIONS

In this work, we developed and validated a gradient descent algorithm that can solve the US calibration problem for various calibration methodologies such as the $AX = XB$ and the $BX^{-1} p$ formulation. In particular, this algorithm enables an on-line update of calibration parameters based on new incoming data. Future work will explore other calibration methodologies, their respective cost functions, and their efficacy within our gradient descent framework.

References

- [1] Boctor, E.M., Stolka, P., Kang, H. J., Clarke, C., Rucker, C., Croom, J., Burdette, E. C., Webster, R. J., III, "Precisely shaped acoustic ablation of tumors utilizing steerable needle and 3D ultrasound image guidance," *SPIE Medical Imaging*, pp. 76252N, 2010.
- [2] Foroughi, P., Csoma, C., Rivaz, H., Fichtinger, G., Zellars, R., Hager, G., Boctor, E.M., "Multi-modality fusion of CT, 3D ultrasound, and tracked strain images for breast irradiation planning," *SPIE*, 72651B, 2009.
- [3] Foroughi P., Rivaz H., Fleming I. N., Hager G. D., and Boctor E. M., "Tracked Ultrasound Elastography (TrUE), *MICCAI*, 9-16, 2010.
- [4] Boctor, E.M., Viswanathan, A., Choti, M.A., Taylor, R.H., Fichtinger, G., Hager, G.D., "A Novel Closed Form Solution for Ultrasound Calibration, *IEEE Int Symp. On Biomedical Imaging*, 527-530, 2004.
- [5] Poon, T., Rohling, R., "Comparison of calibration methods for spatial tracking of a 3-D ultrasound probe." *Ultrasound in Medicine and Biology*, 31(8), 1095-1108, 2005.
- [6] Park, F.C., Martin, B.J., "Robot Sensor Calibration: Solving $AX = XB$ on the Euclidean Group," *IEEE Trans. Robotics and Automation*, 10(5), 717-721, 1994.
- [7] Daniilidis, K., "Hand-Eye Calibration Using Dual Quaternions," *The International Journal of Robotics Research*, 18(3), 286-298, 1999.
- [8] Arun, K.S., Huang, T.S., Blostein, S.D., "Least-Squares Fitting of Two 3-D Point Sets," *IEEE Pattern Analysis and Machine Intel.*, 9(5), 698-700, 1987.
- [9] Chou, J.C.K., Kamel, M., "Finding the Position and Orientation of a Sensor on a Robot Manipulator Using Quaternions," *IJRR*, 10(3), 240-254, 1991.
- [10] Shiu, Y.C., Ahmad, S., "Calibration of Wrist-Mounted Robotic Sensors by Solving Homogeneous Transform Equations of the Form $AX = XB$," *IEEE Trans. Robotics and Automation*, 5(1), 16-29, 1989.
- [11] Prager, R.W., Rohling, R.N., Gee, A.H., Berman, L., "Automatic Calibration for 3-D Free-Hand Ultrasound," *Dep. Eng., Cambridge Univ.*, 1997.
- [12] Melvær, E.L., Mørken, K., Samset, E., "A motion constrained cross-wire phantom for tracked 2D ultrasound calibration," *CARS*, 7(4), 611-620, 2012.
- [13] Cleary, K., Zhang, H., Glossop, N., Levy, E., Wood, B., Banovac, F., "Electromagnetic Tracking for Image-Guided Abdominal Procedures: Overall System and Technical Issues," *IEEE EMBS*, 6748-6753, 2005.
- [14] Chirikjian, G.S., Zhou, S., "Metrics on Motion and Deformation of Solid Models," *ASME Mechanical Design*, 120(2), 252-261, 1998.
- [15] Chirikjian, G.S., Kyatkin, A.B., *Engineering Applications of Noncommutative Harmonic Analysis*, CRC Press, Boca Raton, FL 2001.
- [16] Taylor, C.J., Kriegman, D.J., "Minimization on the Lie group $\text{SO}(3)$ and related manifolds," *Yale Technical Brief*, 1994.
- [17] Lee, S., Fichtinger, G., Chirikjian, G.S., "Novel Algorithms for Robust Registration of Fiducials in CT and MRI," *Medical Physics*, 29(8), 1881-1891, 2002.
- [18] Stein, D., Scheinerman, E.R., Chirikjian, G.S., "Mathematical models of binary spherical-motion encoders," *IEEE/ASME Trans. on Mechatronics*, 8(2), 234-244, 2003.
- [19] Chen, H.H., "A Screw Motion Approach to Uniqueness Analysis of Head-Eye Geometry" *IEEE Conference on Computer Vision and Pattern Recognition*, 1991, 145-151, 1991.
- [20] Ackerman, M.K., Cheng, A., Schiffman, B., Boctor, E.M., Chirikjian, G.S., "Sensor Calibration with Unknown Correspondence: Solving $AX=XB$ Using Euclidean-Group Invariants," *IROS*, 1308-13, 2013.
- [21] Boctor EM, "Enabling Technologies For Ultrasound Imaging In Computer-Assisted Intervention," *Comp. Sci. Dep., Johns Hopkins*, Thesis, 2006.
- [22] Andreff, N., Horaud, R., Espiau, B., 'Robot Hand-Eye Calibration Using Structure-from-Motion" *IJRR*, 20(3), 228-248, 2001.